Journal of Solid State Chemistry 184 (2011) 3195–3201

Contents lists available at SciVerse ScienceDirect

Journal of Solid State Chemistry

journal homepage: www.elsevier.com/locate/jssc

Synthesis and evaluation of lead telluride/bismuth antimony telluride nanocomposites for thermoelectric applications

Shreyashi Ganguly [a,1], Chen Zhou [b,1], Donald Morelli [b,*], Jeffrey Sakamoto [b,*], Ctirad Uher [c,*], Stephanie L. Brock [a,*]

[a] Department of Chemistry, Wayne State University, Detroit, MI 48202, USA
[b] Chemical Engineering and Materials Science, Michigan State University, East Lansing, MI 48824, USA
[c] Physics Department, University of Michigan, Ann Arbor, MI 48109, USA

ARTICLE INFO

Article history:
Received 15 July 2011
Received in revised form
21 September 2011
Accepted 24 September 2011
Available online 5 October 2011

Keywords:
Thermoelectric
Nanocomposite
Incipient wetness
Bismuth telluride
Lead telluride
Semiconductor

ABSTRACT

Heterogeneous nanocomposites of p-type bismuth antimony telluride ($Bi_{2-x}Sb_xTe_3$) with lead telluride (PbTe) nanoinclusions have been prepared by an incipient wetness impregnation approach. The Seebeck coefficient, electrical resistivity, thermal conductivity and Hall coefficient were measured from 80 to 380 K in order to investigate the influence of PbTe nanoparticles on the thermoelectric performance of nanocomposites. The Seebeck coefficients and electrical resistivities of nanocomposites decrease with increasing PbTe nanoparticle concentration due to an increased hole concentration. The lattice thermal conductivity decreases with the addition of PbTe nanoparticles but the total thermal conductivity increases due to the increased electronic thermal conductivity. We conclude that the presence of nanosized PbTe in the bulk $Bi_{2-x}Sb_xTe_3$ matrix results in a collateral doping effect, which dominates transport properties. This study underscores the need for immiscible systems to achieve the decreased thermal transport properties possible from nanostructuring without compromising the electronic properties.

1. Introduction

Thermoelectric (TE) materials are those that can convert heat into electricity or transfer heat by electrical flow. Unlike conventional mechanically driven machines, TE devices use carrier's electrons and holes, to do the work, and thus require no moving parts. Consequently, the efficiency of TE devices is independent of their size and TE devices are reliable, environmentally friendly and suitable for challenging applications such as integrated circuit cooling and power for deep space exploration. However, because of their low efficiency relative to mechanical cycles, TE devices are restricted to niche applications like radioisotope thermoelectric generators (RTGs) for space probes [1]. From a materials perspective, the efficiency of a TE material is determined by its dimensionless figure of merit (FOM), $ZT=S^2\sigma T/\kappa$; where S is the Seebeck coefficient, σ the electrical conductivity, and κ the total thermal conductivity consisting of an electronic part, κ_e, and lattice thermal conductivity, κ_l. The higher a material's ZT, the greater the thermoelectric generation efficiency. The intricate relations among S, σ and κ make seeking high ZT materials hard work because a simple improvement in one parameter typically has an adverse effect on the other(s). Consequently, most conventional bulk TE materials have a $ZT<1$.

Traditional approaches to enhance ZT have focused on optimizing doping to maximize the power factor $S^2\sigma$ [1]. An alternative approach involves decoupling electrical and thermal conductivity by selectively scattering phonons while preserving charge carrier transport [2,3]. In 1993, Hicks and Dresselhaus predicted that the ZT in a 2D quantum well structure could be increased several times over the same 3D bulk materials if superlattice multilayers are properly oriented and their thickness is comparable to the unit cell parameters [3]. Proof of principle experiments in PbTe quantum well structures [4,5], Si/Ge superlattices [6], and Bi_2Te_3/Sb_2Te_3 superlattices [7] demonstrated that a $ZT>1$ is possible. All these findings marked the start of the nanostructure era of TE research.

Several methods have been explored for synthesizing TE nanocomposites. For example, Poudel et al. have reported a $Bi_{2-x}Sb_xTe_3$ nanostructure with a ZT of 1.4 prepared by hot pressing ball-milled nanoparticles into bulk ingots [8]. Also Majumdar and coworkers have observed a reduction in thermal conductivity by a factor of 2 below the alloy limit in crystalline

* Corresponding authors. Fax: +1 313 577 3102.
E-mail addresses: dmorelli@egr.msu.edu (D. Morelli), jsakamot@egr.msu.edu (J. Sakamoto), cuher@umich.edu (C. Uher), sbrock@chem.wayne.edu (S.L. Brock).
[1] These authors contributed equally and are listed in alphabetical order.

0022-4596/$ - see front matter © 2011 Elsevier Inc. All rights reserved.
doi:10.1016/j.jssc.2011.09.031

solids of ErAs nanoparticles incorporated inside $In_{0:53}Ga_{0:47}$ by molecular beam epitaxy [1,9]. Another approach is an *in-situ* synthesis in which nanophases are created by exploiting an inherent phase segregation or decomposition in the alloy or compound system under investigation. For example, the $AgPb_mSbTe_{m+2}$ (LAST-m) family of compounds exhibit a $ZT > 1.5$ due to inhomogeneities on the nanoscale [10]. Recently, Kanatzidis and coworkers have shown that by endotaxially placing SrTe in an Na_2Te-doped PbTe matrix, the thermal conductivity could be reduced and the power factor could be enhanced, achieving a ZT of 1.7 at 800 K [11]. In another example, Zhou et al. has demonstrated a 100% enhancement of ZT in Fe compensated binary skutterudite $Co_{0.9}Fe_{0.1+x}Sb_{3+2x}$ due to the existence of a $FeSb_2$ nanophase [12]. Likewise, in In-filled $CoSb_3$ skutterudites, a significant fraction of indium reacts with Sb to form an *in situ* finely dispersed InSb nanophase in the skutterudite matrix and the combined effect of Ce and In doping results in high performance skutterudite materials with $ZT=1.43$ at 800 K [13].

In this paper, we report a systematic study of the thermoelectric properties of p-type bismuth antimony telluride ($Bi_{2-x}Sb_xTe_3$) based nanocomposites with lead telluride (PbTe) nanoparticles as inclusions. PbTe and $Bi_{2-x}Sb_xTe_3$ were chosen because both components exhibit high ZT as single-phase materials and would benefit from decreased κ_l. We first synthesized discrete PbTe nanoparticles by solution-phase arrested precipitation [14] and bulk matrix $Bi_{2-x}Sb_xTe_3$ by standard solid state synthesis techniques [15]. The nanocomposite was prepared by incipient wetness impregnation, a well-established technique for catalyst production [16]. The method involves addition of solution-dispersed PbTe nanoparticles to the matrix followed by drying. A series of mass fractions of PbTe nanoparticles in bulk $Bi_{2-x}Sb_xTe_3$ were investigated, ranging from 0.1 wt% to 1 wt%. The resulting thermoelectric properties were measured to evaluate the efficacy of our nanocomposite approach for reduction of κ_l.

2. Experimental

2.1. Reagents

Lead acetate trihydrate ($Pb(OAc)_2 \cdot 3H_2O$) was obtained from Baker Chemicals; tellurium powder (Te, 200 mesh, 99.8%), 1-octadecene (ODE, technical grade 90%), hydrazine (anhydrous, 98%) and acetonitrile (anhydrous, 99.8%) were obtained from Aldrich; trioctylphosphine (TOP, technical grade 97%) was obtained from Strem chemicals and oleic acid (OA, technical grade, 90%), hexane and acetone were obtained from Fisher. High purity starting materials of bismuth (granule 99.997%), antimony (shot 99.999%) and tellurium (shot 99.9999%) were obtained from Alfa Aesar.

2.2. Synthesis

2.2.1. General synthesis of PbTe nanoparticles

Discrete PbTe nanoparticles were prepared by combining $Pb(OAc)_2 \cdot 3H_2O$ (1.317 g, 3 mmol) with OA (3 mL, 6 mmol) and ODE (6 mL, 18 mmol) and heating this mixture under inert atmosphere on a Schlenk line at 170 °C for 30 min to obtain a colorless solution [14]. The temperature of the solution was then reduced to 150 °C followed by rapid injection of 3 mL of 1 M TOPTe, which was formed by dissolving 1.27 g of Te in 10 mL of trioctylphosphine solution in a glove box. The resultant solution was left at 150 °C for 5 min and then the reaction was quenched by plunging the flask into a cold-water bath. The nanoparticles were precipitated inside a glove box by adding hexane as the solvent and acetone as the antisolvent, and isolated by centrifugation. Subsequently, the particles were either treated with (1) anhydrous hydrazine or (2) thermal annealing under inert atmosphere (nitrogen atmosphere) in order to remove surface ligands.

2.2.2. General synthesis of p-type bismuth antimony telluride

p-type bismuth antimony telluride with nominal composition $Bi_{0.4}Sb_{1.6}Te_3$ was employed as the matrix material for making nanocomposites. High purity elements were weighed according to the targeted ratio and sealed in a fused silica ampoule under a vacuum $> 10^{-5}$ Torr. The ampoule was heated at 750 °C for 12 h followed by rapid water quenching. The quenched ingot was annealed at 540 °C for another 3 days in order to homogenize the properties. The annealed ingot was ball milled into a fine powder in a Spex 8000 Mixer/Mill and stored inside an Ar purged glovebox before making nanocomposites.

2.2.3. General synthetic procedure for incorporation of PbTe nanoparticles in bulk $Bi_{2-x}Sb_xTe_3$ matrix

The synthesis of nanocomposites involved dispersion of an appropriate mass of PbTe nanoparticles into a minimum amount of solvent, hexane. The resulting solution was sonicated for 10 min to make a colloidal suspension. The PbTe nanoparticle sol was then added dropwise to an appropriate mass of bulk $Bi_{2-x}Sb_xTe_3$ with constant stirring, followed by solvent evaporation under ambient temperature and pressure, in a glove box.

The mixed composite powder was loaded into a graphite crucible and heated at 410 °C for 2 h (in an Ar purged glove box) in order to eliminate residual organics at the surface of the PbTe nanoparticles. The heat treated powder was then hot pressed between 350 °C and 380 °C under a pressure of 60 MPa for 15 min to form a dense pellet. A total of four samples (2 g each) with PbTe weight percentage of 0%, 0.1%, 0.5% and 1% were prepared in this way.

3. Characterization and physical measurements

3.1. Powder X-ray diffraction

Powder X-ray diffraction was collected on a Rigaku RU 200B (40 kV, 150 mA, Cu$K\alpha$ radiation) diffractometer. Samples were deposited on a quartz holder coated with a thin layer of grease and the data were acquired in the 2θ range 20–70° with a step size of 1.2°. The PXRD data obtained were processed using the Jade software package and compared to powder diffraction files (PDFs) from the International Center for Diffraction Data database (ICDD). Least-squares refinement of lattice parameters was achieved using the Jade software package with silicon as an internal standard.

3.2. Transmission electron microscopy and energy dispersive spectroscopy

Transmission electron microscopy (TEM) and energy dispersive spectroscopy (EDS) were performed using a JEOL 2010 transmission electron microscope operated at a voltage of 200 kV and a current of 106–108 μA with a coupled EDS detector (EDAX Inc). Images obtained from TEM measurements were analyzed by Amtv600 software (Advanced Microscopy Techniques Corporation). Samples for TEM were prepared by sonicating PbTe nanoparticles or $PbTe/Bi_{2-x}Sb_xTe_3$ nanocomposites in hexane, followed by deposition of a drop from each solution on a carbon-coated 200 mesh Cu grid (SPI) and air drying for 1 day.

Table 1
Some room temperature (300 K) physical properties of PbTe/$Bi_{2-x}Sb_xTe_3$ nanocomposites.

Sample name	$x=0$ (control)	$x=0.1$	$x=0.5$	$x=1$
PbTe nanoparticles weight percentage	0	0.1	0.5	1
Lattice parameters (Å) and standard deviations	$a=4.2884$ (13) $c=30.459$ (8)	ND	ND	$a=4.2856$ (19) $c=30.443$ (15)
Relative density (%)	95.74	97.09	96.32	94.15
Seebeck coefficient (10^{-6} V/K)	186	136	110	84
Electrical resistivity (mΩ cm)	1.14	0.672	0.688	0.500
Power factor (10^{-6} W cm^{-1}K^{-2})	30.15	26.48	18.11	15.37
Thermal conductivity (10^{-2} W/cm-K)	1.48	1.65	1.71	1.81
Lorenz number (10^{-8} W Ω K^{-2})	1.65	1.78	1.82	2.00
Carrier density (10^{-19} cm^{-3})	3.68	5.41	7.90	10.8

3.3. Infrared spectroscopy

A Varian FTS 3000 MX FTIR spectrometer was used to probe surface organic groups on PbTe nanoparticles and nanocomposites. Powdered samples were ground with KBr and pressed into a transparent pellet in a 13 mm die with 2000 psi pressure from a Carver Hydraulic pellet press.

3.4. Thermogravimetric analysis

Thermogravimetric analysis was performed using a Perkin Elmer, Pyris 1 TGA. PbTe nanoparticles were heated under nitrogen flow from 25 to 700 °C in a ceramic crucible with a temperature ramp rate of 10 °C/min.

3.5. Density measurement

Densities for all hot pressed samples (Table 1) were measured by the Archimedes method with 200 proof ethanol as the fluid medium.

3.6. Thermoelectric transport properties

For thermoelectric transport properties measurement, a rectangular parallelepiped of approximately 2.5 mm × 2.5 mm × 8 mm was cut from the middle of the hot pressed disk using a diamond saw. Seebeck coefficient, electrical resistivity, and thermal conductivity were measured directly in the temperature range 80–380 K under vacuum using a steady state technique in a continuous flow cryostat with liquid nitrogen as a refrigerant. A thin slab of approximately 1 mm thickness was cut from the balance of the disk for Hall measurement. The Hall coefficient was measured in the same temperature range using ac current in a varying magnetic field from −3 T to 3 T in the Quantum Design Versalab system. In order to eliminate complications from anisotropy, all transport properties were measured in the direction perpendicular to the pressing axis. More details on the measurements and instrumentation can be found in Refs. [12,17,18].

4. Results and discussion

4.1. Synthesis

We expected that the presence of uniform PbTe nanoparticles at concentrations of 0.1–1 wt% within a $Bi_{2-x}Sb_xTe_3$ bulk material would result in heterogeneous interfaces that would scatter phonons and thus reduce the thermal conductivity (κ) within the matrix (particularly the lattice portion of the conductivity, κ_l), while having minimal impact on the electrical properties. To achieve a composite, we first prepared PbTe nanoparticles and bulk $Bi_{2-x}Sb_xTe_3$ independently, and then incorporated PbTe into the bulk $Bi_{2-x}Sb_xTe_3$ matrix via incipient wetness impregnation.

p-type $Bi_{2-x}Sb_xTe_3$ was prepared following the literature procedure [15] targeting the composition $Bi_{0.4}Sb_{1.6}Te_3$, where the electrical and thermal characteristics balance to generate the maximum ZT within this homogeneous p-doped alloy. The ball milled powders were characterized by powder X-ray diffraction (PXRD) patterns which were found to match the expected rhombohedral phase of Bi_2Te_3.

Oleate-capped PbTe nanoparticles were synthesized as previously reported [19]. The PXRD patterns match the cubic PbTe (Altaite) phase and have a crystalline thickness of 14 nm based on the Scherrer equation. TEM images reveal that the particles exhibit a cubic morphology with an average particle size of 13 ± 1.2 nm, similar to that obtained by Scherrer analysis, suggesting the particles are fully crystalline. The elemental analysis (EDS) of the as-prepared nanoparticles gives a composition Pb:Te of 1:0.94, close to the ideal value of Pb:Te of 1:1, but with a slight excess of Pb.

4.2. Removal of capping groups from PbTe nanocrystals

The oleate groups terminating the surface of PbTe nanoparticles can be expected to act as insulating barriers, decreasing the overall electrical conductivity of the system [20,21]. Hence, we sought to remove the oleate ligands, exploring both chemical as well as thermal treatments. For the chemical treatments, PbTe nanoparticles dispersed in hexane were treated with anhydrous hydrazine, with stirring, followed by precipitation with acetonitrile, according to a literature procedure [21]. Hydrazine treatment led to some ripening, manifest as a slight increase in the crystallite size from 14 nm to 15 nm (Scherrer analysis of PXRD) as well as significant aggregation (TEM imaging). A comparison of Infrared (IR) spectra obtained before and after hydrazine treatment is shown in Fig. 1. The peaks at 1512 cm^{-1} and 1394 cm^{-1} are attributed to the presence of symmetric and asymmetric stretching vibrations of oleate COO^-, respectively, whereas those at 2918 cm^{-1} and 2840 cm^{-1} correspond to oleate aliphatic –CH stretches. While significant reduction in peak intensity is observed upon hydrazine treatment, the IR data suggest that complete removal is not achieved.

Thermal treatment was found to be more effective for oleate group removal. A suitable temperature was determined by employing thermogravimetric analysis (TGA), under nitrogen atmosphere. As shown in Fig. 2, the TGA of the oleate-capped PbTe nanoparticles revealed a 16% weight loss overall between 255 and 455 °C, which we attribute to desorption/decomposition of surface oleate functionalities as well as possible loss of Te due

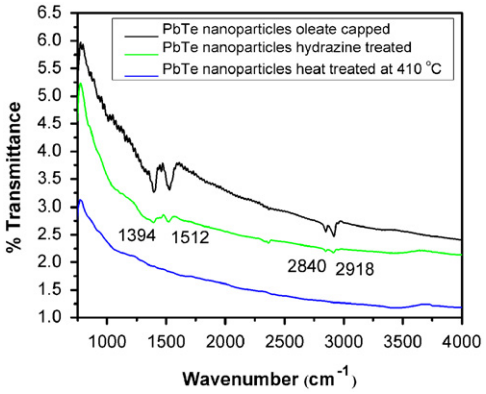

Fig. 1. IR of as-prepared PbTe nanoparticles, PbTe nanoparticles chemically treated with hydrazine, and PbTe nanoparticles thermally treated under Ar in a flow furnace at 410 °C.

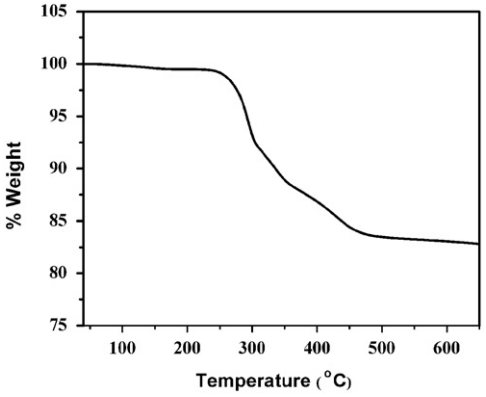

Fig. 2. TGA of PbTe oleate-capped nanoparticles under N_2 atmosphere.

to sublimation at the high temperature end of the measurement. However, the loss of Te is expected to be less than 1 wt% under these conditions [22]. Based on the TGA data, heat treatment of the nanoparticles was carried out in a flow furnace at 410 °C for 2 h under nitrogen. As shown in Fig. 1, both –COOH and –CH stretching vibrations are absent after thermal treatment, suggesting successful removal of the organic groups.

4.3. Nanocomposite preparation

In order to avoid aggregation and particle growth during the thermal ligand removal step, and to enable the most efficient and intimate mixing between the nanoparticles and the matrix, the incorporation of nanoparticles into bulk $Bi_{2-x}Sb_xTe_3$ was achieved by the addition of a dispersion of oleate-capped PbTe nanoparticles in hexane to solid $Bi_{2-x}Sb_xTe_3$ dropwise, with constant stirring of the slurry to facilitate incorporation of the PbTe nanoparticles throughout the $Bi_{2-x}Sb_xTe_3$ matrix, then left to dry under inert atmosphere. The resultant composite was then placed inside a carbon crucible, in an Ar purged glovebox, and heated at 410 °C for 2 h to pyrolyze organic ligands encapsulating the PbTe nanoparticles. The heat treated powder was then hot pressed inside a 10 mm graphite die under a pressure of 60 MPa at an approximate temperature of 350 °C to 390 °C for 15 min. A total of three nanocomposites with 0.1 wt%, 0.5 wt% and 1 wt% PbTe nanoparticles were prepared. A pure bismuth antimony telluride matrix material was hot pressed under identical conditions to serve as a control sample.

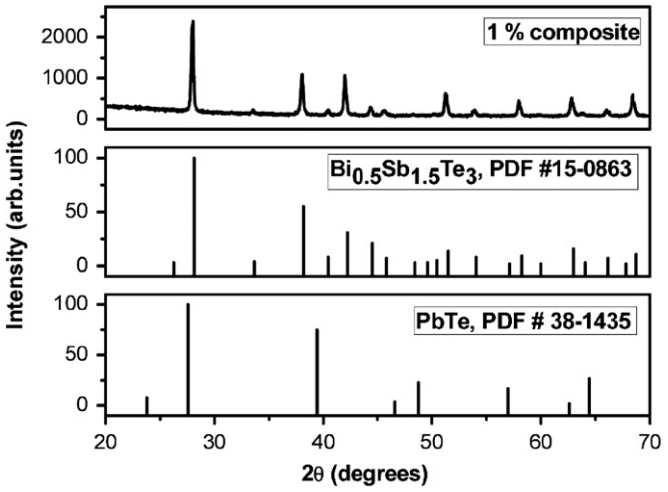

Fig. 3. PXRD of 1 wt% PbTe nanoparticles in $Bi_{2-x}Sb_xTe_3$ matrix (after compaction). The patterns are referenced to the ICDD-PDF # 38-1435 of cubic PbTe and ICDD-PDF # 15-0863 of rhombohedral Bi_2Te_3.

PbTe nanoparticles within the $Bi_{2-x}Sb_xTe_3$ nanocomposite cannot be detected by PXRD at the low concentrations explored here (Fig. 3) due to limitations in the sensitivity of the PXRD technique. Incorporation did not have an effect on the lattice parameters, which were found to be the same within 2σ (Table 1) for comparison of the matrix to the highest doped material (1 wt%). However, this observation does not rule out solid-solution formation since the doping levels are small and minimal changes in lattice parameter are expected. Confirmation that PbTe nanoparticles remain intact is provided by TEM images. Fig. 4 shows the images of the precursor nanoparticles as well as composites of 1 wt%, 0.5 wt% and 0.1 wt% of PbTe nanoparticles in the $Bi_{2-x}Sb_xTe_3$ matrix after hot pressing the nanocomposites. The presence of higher contrast 12–13 nm sized cubes similar to those seen in the discrete PbTe nanoparticle samples is evident in all images, with fewer detected at lower concentrations inside the lighter contrast $Bi_{2-x}Sb_xTe_3$ matrix. The presence of PbTe nanoparticles was evident throughout the matrix in all cases and showed no agglomeration, suggesting good dispersion.

4.4. Transport properties

For the sake of simplicity, we use the weight percentage, x, of PbTe nanoparticles to identify our samples. Table 1 lists some of the room temperature physical properties of the hot pressed nanocomposites.

Fig. 5 displays the temperature dependence of electronic properties for our nanocomposite samples as well as the control sample, $x=0$. The Seebeck coefficients of nanocomposites decrease monotonously with increasing concentration of PbTe nanoparticles. The electrical resistivity exhibits the same trend, except that $x=0.1$ and 0.5 have nearly identical resistivity. Despite the decrease in resistivity the thermoelectric power factors ($S^2\sigma$) of nanocomposites are lower than the control sample due to the much stronger contribution of the Seebeck coefficient.

Fig. 6 shows the corresponding thermal conductivity data as a function of temperature. The lattice thermal conductivity κ_l shown in the inset of Fig. 6 was calculated by subtracting the electronic thermal conductivity κ_e from the total thermal conductivity. The electronic thermal conductivity is estimated by using the Wiedemann–Franz law, $\kappa_e = L\sigma T$; where L is the Lorenz number, σ the electrical conductivity and T the absolute

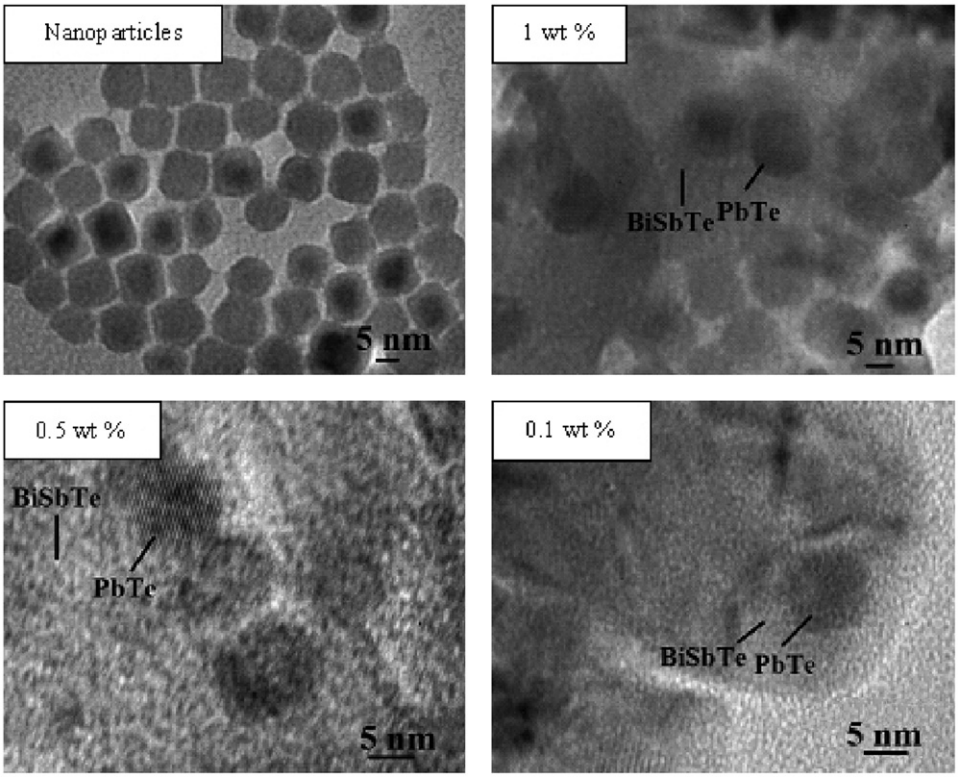

Fig. 4. TEM images of discrete PbTe nanoparticles, 1 wt%, 0.5 wt% and 0.1 wt% PbTe nanoparticles in $Bi_{2-x}Sb_xTe_3$ (BiSbTe) nanocomposites, after hot pressing.

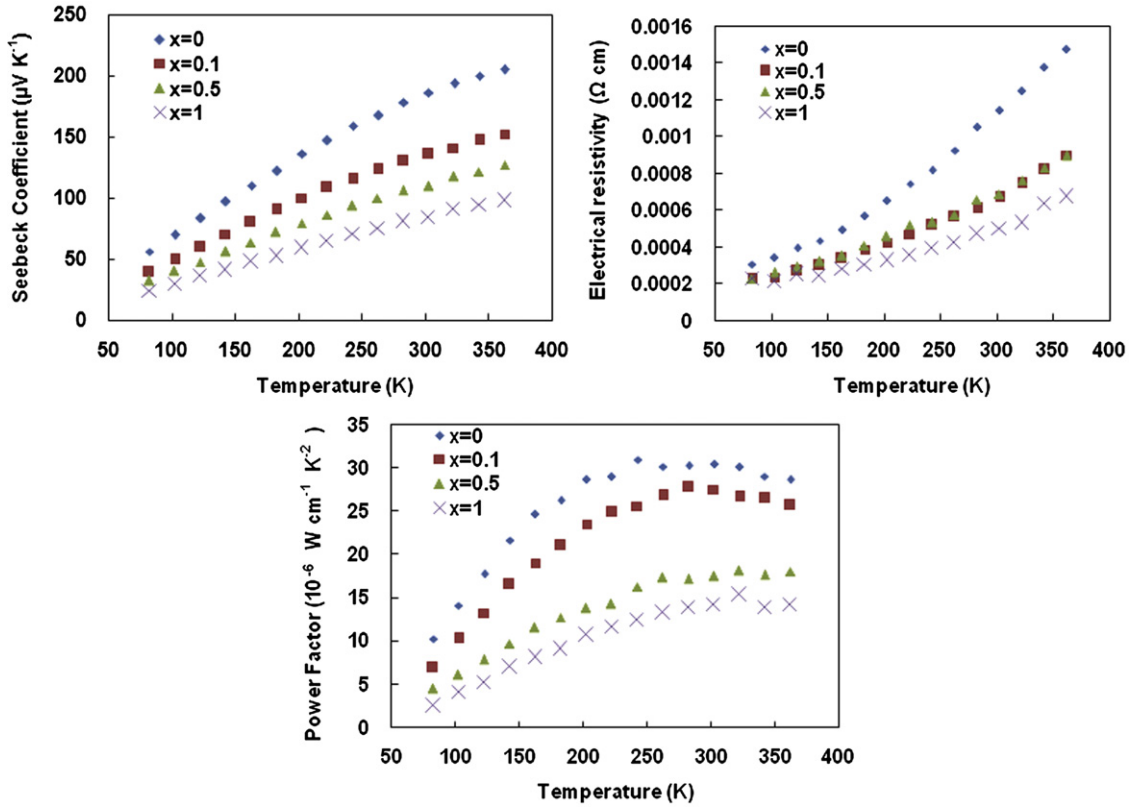

Fig. 5. Electronic properties of nanocomposites as a function of temperature.

temperature. The choice of a reasonable Lorenz number is a delicate issue as we cannot assume our samples to be degenerate semiconductors. We also note that there is approximately a factor of three difference between the most resistive and least resistive samples, so one Lorenz number may not fit all the data equally well. To tackle this problem, we first estimated the reduced Fermi

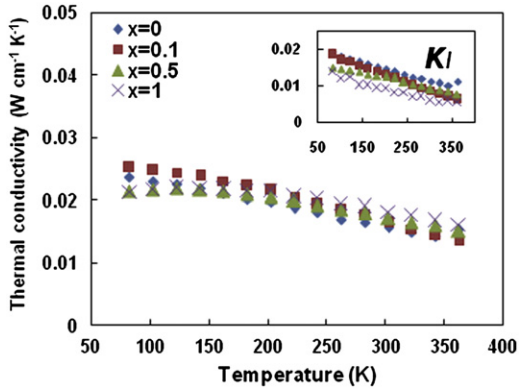

Fig. 6. Thermal conductivity as a function of temperature. The inset shows the lattice thermal conductivity as a function of temperature.

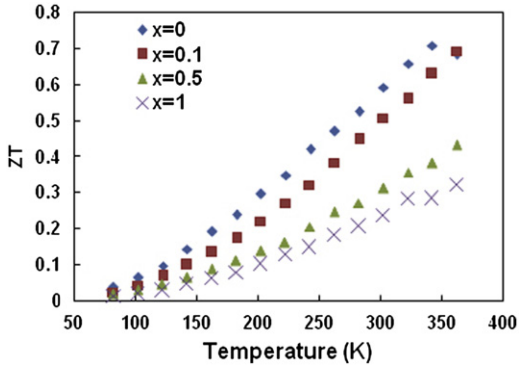

Fig. 7. Dimensionless thermoelectric Figure of Merit, ZT, as a function of temperature.

energy η from the Seebeck coefficient by

$$S = \mp \frac{k}{e}\left\{\frac{((5/2)+\lambda)F_{(3/2)+\lambda}}{((3/2)+\lambda)F_{(1/2)+\lambda}} - \eta\right\} \quad (1)$$

where k is the Boltzmann constant, λ is the exponent of energy in the scattering law, $\tau \sim E^{\lambda}$ and F is the Fermi–Dirac integral given by

$$F_r = \int_0^{\infty} \frac{\xi^r}{1+\exp(\xi-\eta)}\, d\xi \quad (2)$$

where ξ is the reduced kinetic energy of the carriers. For this study, we use $\lambda = -0.5$ in Eq. (1), a value typically used for acoustic phonon scattering of carriers, to estimate the reduced Fermi energy, η. From η we calculated the Lorenz number by

$$L = \frac{3F_0F_2 - 4F_1^2}{F_0^2}\left(\frac{k}{e}\right)^2 \quad (3)$$

A more detailed description of the above analysis can be found in Ref. [23]. We repeated this process for each sample in order to get a more accurate estimation of the Lorenz number (see Table 1) and hence the lattice thermal conductivity. We found that, despite an overall increase in total thermal conductivity, the nanocomposite samples exhibit a reduced lattice thermal conductivity compared to the control sample, as expected if the nanoscale interfaces are acting to scatter phonons. The lattice thermal conductivity of sample $x=1$ is reduced by close to 50% compared to the control sample. Thus, it appears that the overall increase in thermal conductivity can be attributed to the increase in electrical conductivity causing an increase in κ_e.

Fig. 7 shows the dimensionless thermoelectric Figure of Merit, ZT, as a function of temperature. ZTs of nanocomposites are reduced compared to matrix $Bi_{2-x}Sb_xTe_3$, with the strongest contributing factor the decreased Seebeck coefficient. A significant ZT reduction starts at PbTe wt% as little as 0.5.

In order to discern the origin of the strong electronic effects noted upon PbTe nanoparticle incorporation, carrier concentration was measured as a function of temperature (Fig. 8). The hole concentration increases with increasing PbTe concentration, suggesting the incorporation of PbTe nanoparticles is also introducing a p-type dopant. This is consistent with the work by Kusano and coworkers, who have attempted to mechanically alloy bulk $Bi_{2-x}Sb_xTe_3$ and PbTe and consolidated the powder by spark plasma sintering. The TE transport properties of the resultant composites exhibited a similar trend as in our study and they concluded the increase of carrier concentration is due to a doping effect associated with PbTe [24]. This doping was attributed to either the effect of PbTe as an inclusion, since PbTe is generally a p-type semiconductor, or from Pb^{2+} leaching from the incorporated nanoparticles and occupying Bi^{3+} sites within the matrix, generating a hole, and thus increasing the overall hole concentration [24]. The transport of Pb^{2+} from the PbTe particles to the bulk matrix may arise in part from Te sublimation during the ligand removal step. Pb has also been used as a p-type dopant for both Bi_2Te_3 and Sb_2Te_3, as reported by Plecháček et al. where they concluded that the increase of hole concentration arises from the interaction between Pb atoms and native point defects (antisite defects or Te vacancies) in Bi_2Te_3 and Sb_2Te_3 [25,26].

To further elucidate the effect of PbTe nanoparticle incorporation on the properties of the $Bi_{2-x}Sb_xTe_3$ matrix, we plot the Pisarenko relation of p-type $Bi_{2-x}Sb_xTe_3$ and PbTe/$Bi_{2-x}Sb_xTe_3$ nanocomposites (Fig. 9). The fit line is created from a number of $Bi_{0.4}Sb_{1.6}Te_3$ samples (created in the Sakamoto lab), each

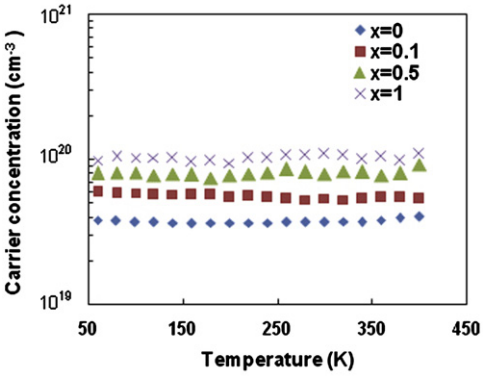

Fig. 8. Temperature dependence of carrier concentration.

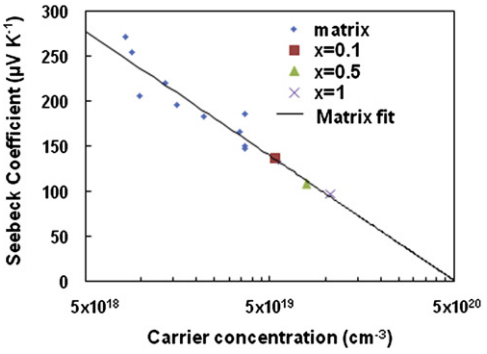

Fig. 9. Pisarenko relation of nanocomposites. The fitted line is constructed as an aid to guide the eye. All matrix bismuth antimony telluride with various carrier concentrations were synthesized in the Sakamoto lab.

displaying a different carrier concentration. From the approximate Eq. (4) (based on a simplified one carrier model [18]), for a series of samples that share the same exponent of scattering, λ, and approximately the same effective mass, m^*, the Seebeck coefficient is proportional to the logarithmic inverse of the carrier concentration (n_p) and should thus fall close to the fitted line in a Pisarenko relation plot

$$S \propto \frac{k}{e}\left(\lambda + \text{const} + \ln\frac{2(2\pi m^* kT)^{3/2}}{h^3 n_p}\right) \quad (4)$$

As shown in Fig. 9, the points representing nanocomposites fall in the vicinity of the fitted line, suggesting that the charge carrier scattering mechanism for nanocomposites is the same as for matrix materials (if we assume m^* is not affected by the low percentage of PbTe incorporation). Thus, the enhanced carrier concentration appears to be due to incorporation of Pb^{2+} in the $Bi_{2-x}Sb_xTe_3$ matrix, resulting in a decreased Seebeck coefficient, decreased resistivity, and increased κ_e. The presence of Pb^{2+} ions within the $Bi_{2-x}Sb_xTe_3$ matrix may also contribute to reduced lattice conductivity; decreased κ_l in antimony telluride doped with lead telluride has been attributed to an ion-doping effect [27].

5. Conclusion

As a means to reduce lattice thermal conductivity in p-type $Bi_{2-x}Sb_xTe_3$ for improved thermoelectrics, the incorporation of discrete, monodisperse 13 nm PbTe nanoparticle "scattering centers" was achieved using an incipient wetness approach. Thermal-treatment of the resultant composite is effective at removing residual surface ligands from the nanoparticle preparation, and the presence of PbTe cubes within the matrix is evident after both the ligand removal (410 °C) and hot-pressing (350–380 °C) steps. Evaluation of the thermoelectric properties of the PbTe/$Bi_{2-x}Sb_xTe_3$ composites for PbTe nanoparticle loadings of between 0.1% and 1% reveal a decrease in Seebeck coefficient and in electrical resistivity, attributed to an increase in hole carrier concentration. Based on the behavior of the $Bi_{2-x}Sb_xTe_3$ matrix for different carrier concentrations (Pisarenko relation), relative to the nanocomposites, it can be concluded that the carrier scattering mechanism is the same in each, i.e., the electrical properties arise from incorporation of Pb^{2+} from the PbTe nanoparticles into the $Bi_{2-x}Sb_xTe_3$ matrix. As expected, the lattice thermal conductivity decreases with the addition of PbTe nanoparticles but this effect is small and countermanded by the changes in Seebeck, and κ_e. Moreover, in the present system we cannot differentiate between phonon scattering at nanoparticle interfaces or at defects due to Pb incorporation within the $Bi_{2-x}Sb_xTe_3$ matrix. Future studies will be focused on immiscible systems in order to tune the thermal transport properties without negatively impacting the electronic properties due to doping.

Acknowledgments

This material is based upon work supported as part of *Revolutionary Materials for Solid State Energy Conversion*, an Energy Frontier Research Center funded by the U.S. Department of Energy, Office of Science, and Office of Basic Energy Sciences under Award no. DE-SC0001054, and also by the University Research Corridor. Electron microscopy was acquired in the WSU Central Instrumentation Facility on a JEOL 2010 purchased under NSF Grant DMR-0216084.

References

[1] M.S. Dresselhaus, G. Chen, M.Y. Tang, R. Yang, H. Lee, D. Wang, Z. Ren, J.-P. Fleurial, P. Gogna, Adv. Mater. 19 (2007) 1043–1053.
[2] L.D. Hicks, M.S. Dresselhaus, Phys. Rev. B Condens. Matter 47 (1993) 16631–16634.
[3] L.D. Hicks, M.S. Dresselhaus, Phys. Rev. B Condens. Matter 47 (1993) 12727–12731.
[4] L.D. Hicks, T.C. Harman, X. Sun, M.S. Dresselhaus, Phys. Rev. B Condens. Matter 53 (1996) R10493–R10496.
[5] T.C. Harman, D.L. Spears, M.J. Manfra, J. Electron. Mater. 25 (1996) 1121–1127.
[6] T. Koga, S.B. Cronin, M.S. Dresselhaus, J.L. Liu, K.L. Wang, Appl. Phys. Lett. 77 (2000) 1490–1492.
[7] R. Venkatasubramanian, E. Siivola, T. Colpitts, B. O'Quinn, Nature 413 (2001) 597–602.
[8] B. Poudel, Q. Hao, Y. Ma, Y. Lan, A. Minnich, B. Yu, X. Yan, D. Wang, A. Muto, D. Vashaee, X. Chen, J. Liu, M.S. Dresselhaus, G. Chen, Z. Ren, Science 320 (2008) 634–638.
[9] W. Kim, J. Zide, A. Gossard, D. Klenov, S. Stemmer, A. Shakouri, A. Majumdar, Phys. Rev. Lett. 96 (2006) 045901.
[10] J.R. Sootsman, D.Y. Chung, M.G. Kanatzidis, Angew. Chem. Int. Ed. 48 (2009) 8616–8639.
[11] K. Biswas, J. He, Q. Zhang, G. Wang, C. Uher, V.P. Dravid, M.G. Kanatzidis, Nat. Chem. 3 (2011) 160–166.
[12] C. Zhou, J. Sakamoto, D. Morelli, X. Zhou, G. Wang, C. Uher, J. Appl. Phys. 109 (2011) 063722/1–063722/5.
[13] H. Li, X. Tang, Q. Zhang, C. Uher, Appl. Phys. Lett. 94 (2009) 102114/1–102114/3.
[14] S. Ganguly, S.L. Brock, J. Mater. Chem. 21 (2011) 8800–8806.
[15] L. Chen, J. Jiang, X. Shi, Mater. Res. Soc. Symp. Proc. 793 (2004) 365–373.
[16] E.L. Lee, I.E. Wachs, J. Phys. Chem. C 112 (2008) 20418–20428.
[17] E. Skoug, C. Zhou, Y. Pei, D.T. Morelli, Appl. Phys. Lett. 94 (2009) 022115/1–022115/3.
[18] A.F. Ioffe, Semiconductor Thermoelements, and Thermoelectric Cooling, Infosearch Ltd, 1957.
[19] J.E. Murphy, M.C. Beard, A.G. Norman, S.P. Ahrenkiel, J.C. Johnson, P. Yu, O.I. Micic, R.J. Ellingson, A.J. Nozik, J. Am. Chem. Soc. 128 (2006) 3241–3247.
[20] D.V. Talapin, C.B. Murray, Science 310 (2005) 86–89.
[21] M. Law, J.M. Luther, Q. Song, B.K. Hughes, C.L. Perkins, A.J. Nozik, J. Am. Chem. Soc. 130 (2008) 5974–5985.
[22] S. Yoneda, M. Kato, I.J. Ohsugi, J. Appl. Phys. 107 (2010) 074901/1–074901/6.
[23] H.J. Goldsmid, Applications of Thermoelectricity, John Wiley & Sons Inc., New York, 1960.
[24] D. Kusano, Y. Hori, in: 21st International Conference on Thermoelectrics, 2002, pp. 13–16.
[25] T. Plecháček, J. Horák, J. Solid State Chem. 145 (1999) 197–203.
[26] T. Plecháček, J. Navrátil, J. Horák, P. Lošťák, Philos. Mag. 84 (2004) 2217–2228.
[27] P.-W. Zhu, Y. Imai, Y. Isoda, Y. Shinohara, X.-P. Jia, G.-T. Zou, Chin. Phys. Lett. 22 (2005) 2103–2105.